Mon. Not. R. Astron. Soc. **396,** 1297–1307 (2009) doi:10.1111/j.1365-2966.2009.14823.x

LoCuSS: luminous infrared galaxies in the merging cluster Abell 1758 at $z = 0.28$

C. P. Haines,[1⋆] G. P. Smith,[1] E. Egami,[2] N. Okabe,[3] M. Takada,[4] R. S. Ellis,[5,6] S. M. Moran[7] and K. Umetsu[8,9]

[1]*School of Physics and Astronomy, University of Birmingham, Edgbaston, Birmingham B15 2TT*
[2]*Steward Observatory, University of Arizona, 933 North Cherry Avenue, Tucson, AZ 85721, USA*
[3]*Astronomical Institute, Tohoku University, Aramaki, Aoba-ku, Sendai 980-8578, Japan*
[4]*Institute of Physics and Mathematics of the Universe, The University of Tokyo, 5-1-5 Kashiwa-no-Ha, Kashiwa City, Chiba 277-8582, Japan*
[5]*California Institute of Technology, 105-24 Astronomy, Pasadena, CA 91125, USA*
[6]*Department of Astrophysics, University of Oxford, Keble Road, Oxford OX1 3RH*
[7]*Department of Physics and Astronomy, The Johns Hopkins University, 3400 N. Charles Street, Baltimore, MD 21218, USA*
[8]*Institute of Astronomy and Astrophysics, Academica Sinica, PO Box 23-141, Taipei 106, Taiwan*
[9]*Leung Center for Cosmology and Particle Astrophysics, National Taiwan University, Taipei 10617, Taiwan*

Accepted 2009 March 24. Received 2009 March 24; in original form 2008 December 12

ABSTRACT

We present the first galaxy evolution results from the Local Cluster Substructure Survey (LoCuSS), a multiwavelength survey of 100 X-ray selected galaxy clusters at $0.15 \leq z \leq 0.3$. LoCuSS combines far-ultraviolet (UV) through far-infrared (IR) observations of cluster galaxies with gravitational lensing analysis and X-ray data to investigate the interplay between the hierarchical assembly of clusters and the evolution of cluster galaxies. Here we present new panoramic *Spitzer*/Multiband Imaging Photometer 24-μm observations of the merging cluster Abell 1758 at $z = 0.279$ spanning $6.5 \times 6.5\,\mathrm{Mpc}^2$ and reaching a 90 per cent completeness limit of $S_{24\,\mu\mathrm{m}} = 400\,\mu\mathrm{Jy}$. We estimate a global cluster star formation rate of $\mathrm{SFR}_{24\,\mu\mathrm{m}} = 910 \pm 320\,\mathrm{M}_{\odot}\,\mathrm{yr}^{-1}$ within $R < 3\,\mathrm{Mpc}$ of the cluster centre, originating from 42 galaxies with $L_{8-1000\,\mu\mathrm{m}} > 5 \times 10^{10}\,\mathrm{L}_{\odot}$. The obscured activity in A1758 is therefore comparable with that in Cl 0024+1654, the most active cluster previously studied at 24 μm. The obscured galaxies faithfully trace the cluster potential as revealed by the weak-lensing mass map of the cluster, including numerous mass peaks at $R \sim 2$–$3\,\mathrm{Mpc}$ that are likely associated with infalling galaxy groups and filamentary structures. However, the core ($R \lesssim 500\,\mathrm{kpc}$) of A1758N is ∼two times more active in the IR than that of A1758S, likely reflecting differences in the recent dynamical history of the two clusters. The 24-μm results from A1758 therefore suggest that dust-obscured cluster galaxies are common in merging clusters and suggest that obscured activity in clusters is triggered by both the details of cluster–cluster mergers and processes that operate at larger radii including those within in-falling groups. Our ongoing far-UV through far-IR observations of a large sample of clusters should allow us to disentangle the different physical processes responsible for triggering obscured star formation in clusters.

Key words: galaxies: active – galaxies: clusters: general – galaxies: evolution – galaxies: stellar content.

1 INTRODUCTION

Unravelling the physics of how gas-rich disc galaxies, recently arrived in galaxy clusters, are transformed into the quiescent elliptical and S0 populations that dominate dense cluster cores at $z \simeq 0$ is one of the longest standing unsolved problems in astrophysics. Numerous studies of massive early-type galaxies in clusters have revealed predominately old stellar populations with apparently very little growth in stellar mass in massive cluster galaxies since $z \sim 1$ (Tanaka et al. 2005; De Propris et al. 2007; Muzzin et al. 2008). This indicates that the majority of stars in cluster early-type galaxies formed at high redshift, $z \gtrsim 2$. However, Butcher & Oemler (1978, 1984) found that the fraction of cluster members with blue optical

⋆E-mail: cph@star.sr.bham.ac.uk

colours increases from zero in the local Universe to ∼0.2 by $z \simeq 0.4$, suggesting that the fraction of cluster galaxies that are actively forming stars increases with increasing lookback time. Empirically the star-forming spiral galaxies found by Butcher & Oemler (1978, 1984) at $z \sim 0.2$–0.4 are mostly replaced by S0 galaxies in local clusters (Dressler 1980; Dressler et al. 1997; Treu et al. 2003). Indeed, S0s may be completely absent at $z \simeq 1$ (Smith et al. 2005), although Desai et al. (2007) suggest that the S0 fraction remains constant over $0.5 < z < 1$ (see also Postman et al. 2005). A simple interpretation is that clusters accrete blue gas-rich star-forming spirals at $z \geq 0.5$–1 and that these galaxies were transformed somehow into the passive S0s found in local clusters.

Numerous mechanisms have been proposed to deplete the reservoir of gas in late-type spiral galaxies and thus cut off the fuel supply for further star formation, leading to transformation into S0 galaxies (for reviews see Boselli & Gavazzi 2006; Haines et al. 2007). Historically most of the work on this area has concentrated on optical wavelengths, for example identifying the so-called E+A galaxies (Poggianti et al. 1999). These galaxies exhibit deep Balmer absorption lines and lack nebular emission lines indicating that these apparently passive galaxies were actively forming stars in the preceding ∼0.5–1.5 Gyr. Indeed, simple evolutionary models have been used to connect, via aging and thus fading, this newly quiescent population with actively star-forming spiral galaxies.

Mid-infrared (MIR) observations of cluster galaxies with *ISO* (*Infrared Space Observatory*) and *Spitzer* have challenged the idea that all spiral galaxies that fall into clusters simply fade into passive galaxies via an intermediate E+A phase. For example, *ISO* revealed a population of luminous infrared galaxies (LIRGs; $L_{\rm IR} \geq 10^{11}\,{\rm L}_{\odot}$) and near-LIRGs in clusters that imply that the star formation rates (SFRs) derived from optical diagnostics (e.g. [O II]) underestimate the true SFR by ∼10–30 times (see Metcalfe, Fadda & Biviano 2005, for a review). Deep radio observations have also revealed that many E+As harbour significant ongoing star formation missed by optical diagnostics due to heavy dust obscuration (Smail et al. 1999; Miller & Owen 2003; Miller, Oegerle & Hill 2006). The simple optically derived fading of spiral galaxies therefore seems to be substantially incomplete.

Radio and MIR observations have also revealed an order of magnitude cluster-to-cluster variations in the amount of obscured star formation in clusters (Owen et al. 1999; Fadda et al. 2000; Duc et al. 2002, 2004; Metcalfe et al. 2003; Miller & Owen 2003; Biviano et al. 2004; Coia et al. 2005a,b; Geach et al. 2006; Bai et al. 2007; Marcillac et al. 2007; Saintonge, Tran & Holden 2008; Dressler et al. 2009; Gallazzi et al. 2009). These differences have broadly been attributed to differences in the recent dynamical history of the clusters (e.g. Owen et al. 1999; Miller & Owen 2003; Geach et al. 2006), however, early *ISO* results had already suggested that a simple one-to-one relationship between cluster–cluster mergers and obscured star formation does not exist. For example, *ISO* identified 10 LIRGs in Cl 0024 and none in A1689, A2218 and A2390 (Coia et al. 2005b; see also Metcalfe et al. 2005). All four clusters are well known strong lensing clusters, the mass distributions of which are constrained by their strong lensing signal to be multimodal, i.e. indicative of recent cluster–cluster merging (e.g. Kneib et al. 1996; Czoske et al. 2002; Swinbank et al. 2006; Limousin et al. 2007).

Indications of the likely complex relationship between the dynamical state of clusters and their current SFR were also found in the pioneering optical studies. For example, for the Coma cluster Caldwell et al. (1993) found numerous galaxies with post-starburst characteristics (strong Balmer-line absorption) between the two X-ray peaks corresponding to the main Coma cluster and the NGC 4839 subcluster, suggestive of starbursts and subsequent quenching resulting from a cluster–cluster merger. In contrast, Tomita et al. (1996) found no enhancement in the blue galaxy distribution between the two X-ray peaks for an apparently similar system Abell 168. For this latter case, Tomita et al. (1996) suggest that the lack of enhanced star formation could be due to the galaxies being previously gas poor and hence unable to be triggered on interaction with their environment. Butcher & Oemler (1984) measured the fraction of cluster galaxies with blue optical colours out to $z \simeq 0.5$, although their sample was dominated by clusters at $0.15 \leq z \leq 0.3$. The blue galaxy fractions in these 'intermediate' redshift clusters span the full range of values found in clusters at $z \simeq 0$ and 0.5, i.e. $f_{\rm B} \sim 0$–0.2. Numerous ultraviolet (UV)/optical, infrared (IR) and radio surveys have broadly confirmed that the scatter is large, however, none have combined the sample size and multiwavelength data set required to relate directly actively star-forming galaxies in clusters to differences in the intracluster medium (ICM) and recent dynamical history of clusters.

The Local Cluster Substructure Survey (LoCuSS; PI: G. P. Smith; http://www.sr.bham.ac.uk/locuss) is a systematic multiwavelength survey of 100 galaxy clusters at $0.15 \leq z \leq 0.3$ drawn from the *ROSAT* All Sky Survey cluster catalogues (Ebeling et al. 1998, 2000; Böhringer et al. 2004). The overall goal of the survey is to probe the relationship between the recent hierarchical infall history of clusters (as revealed by strong and weak lensing observations; Smith & Taylor 2008) and the baryonic properties of the clusters. This results in two complementary aspects of the survey: mass–observable scaling relations (Zhang et al. 2008), and evolution of cluster galaxy populations. Both of these themes are connected by the aim of measuring and understanding the physical origin of the cluster-to-cluster scatter.

This is the first in a series of papers about the first batch of 31 clusters observed by LoCuSS, for which the following data have been gathered: wide-field Subaru/Suprime-CAM imaging, *Hubble Space Telescope* Wide-Field Planetary Camera 2 (WFPC2) and/or Advanced Camera for Surveys (ACS) imaging of the cluster cores, wide-field *Spitzer*/Multiband Imaging Photometer (MIPS) 24-μm maps to match the half-degree Suprime-CAM field of view, *GALEX* near-/far-ultraviolet (NUV/FUV) imaging and wide-field near-infrared (NIR) imaging obtained via a combination of United Kingdom Infrared Telescope (UKIRT)/Wide Field Camera (WFCAM) and KPNO-4m/NEWFIRM. We have also been awarded 500 ks on *Herschel* as an Open Time Key Program to observe this sample at 100 and 160 μm with Photodetector Array Camera and Spectrometer (PACS). The galaxy evolution goals that we will tackle with these data include to measure robustly the scatter in the amount of obscured star formation in clusters at 'low' redshift (Haines et al. 2009), and to cross-correlate the location of the obscured cluster galaxies with mass–overdensities found in the weak-lensing mass maps derived from the Subaru data (Okabe & Umetsu 2008; Okabe et al. 2009). Full details of the survey design will be given in a future paper, however, here we emphasize that at the nominal redshift of our sample, $z = 0.2$, the Suprime-CAM field-of-view covers $6 \times 6\,{\rm Mpc}^2$ centred on each cluster. A $10^{15}\,{\rm M}_{\odot}$ Navarro, Frenk & White (1997) dark matter halo has a virial radius of $r_{200} \simeq 1.7$ Mpc. Our survey therefore probes out to ∼1.5–2 times the virial radius of the clusters. The UV and IR data discussed above all cover at least the same field of view as the Subaru data. This survey is therefore sensitive to the infall regions of clusters studied recently by, for example, Geach et al. (2006) and Moran et al. (2007).

In this paper we present an analysis of Abell 1758 (A1758) at $z = 0.279$ as a case study on the influence of cluster–cluster mergers on obscured star formation, and to outline the methods that will be applied to the full sample in future papers. A1758 was selected for this study because previous X-ray and lensing studies have identified it as a merging cluster, comprising two gravitationally bound components – one to the north and one to the south (A1758N and A1758S, respectively) – both of which are undergoing a merger (David & Kempner 2004; Okabe & Umetsu 2008). We note that throughout the paper, we describe the star formation measured from the 24-μm data as obscured, making no distinction between heavily obscured star formation or the much less attenuated diffuse emission from normally star-forming spirals as done by Gallazzi et al. (2009). The most straightforward interpretation (Kennicutt et al. 2007) of the 24-μm emission is that it traces the dust-obscured star formation, while the observed UV or Hα emission traces the unobscured one (Calzetti et al. 2007). In future, we will combine UV and IR data to obtain robust measures of both obscured and unobscured star formation in cluster galaxies, as well as the level of extinction.

In Section 2 we describe our observations of A1758, plus archival data from the XMM-LSS field that we use to establish optimal colour selection criteria to identify galaxies at the cluster redshift. In Sections 3 and 4 we present the photometric analysis and the main results, respectively. We discuss the results in Section 5 and summarize them in Section 6. When necessary we assume $\Omega_{\rm M} = 0.3$, $\Omega_\Lambda = 0.7$ and $H_0 = 70\,{\rm km\,s^{-1}\,Mpc^{-1}}$, giving a look-back time of 3.3 Gyr and an angular scale of 260 kpc arcmin^{-1} at the cluster redshift. All magnitudes are quoted in the Vega system unless otherwise stated.

2 DATA

2.1 Observations of A1758

The 24-μm data were obtained with MIPS (Rieke et al. 2004) on board the *Spitzer Space Telescope*[1] (Werner et al. 2004), and consist of two separate AORs observed on 2008 January 6 and May 17 (PID:40872, PI: G. P. Smith). The pointing centres of the two AORs are separated by 6 arcmin, each covering a field of view of $25 \times 25\,{\rm arcmin^2}$ with a 5×5 grid. In the earlier AOR, the central pointing was excluded by using the fixed cluster mode (with 400-arcsec offsets) since the area had already been imaged by a Guaranteed Time Observations program 83 to a much deeper depth ($\sim$3000 s pixel^{-1}). However, the second AOR uses the raster mode (i.e. with no gaps), and as a result, it contains the GTO area as well. For both the fixed cluster and raster AORs, we performed at each grid point two cycles of the small-field photometry observations with a frame time of 3 s, producing a per pixel exposure of 90 s for each AOR, or 180 s in the overlapping region.

The 24-μm data were reduced and combined with the Data Analysis Tool (DAT) developed by the MIPS instrument team (Gordon et al. 2005). A few additional processing steps were also applied as described in Egami et al. (2006). The data were resampled and mosaicked with half of the original instrument pixel scale (1.245 arcsec) to improve the spatial resolution.

The clusters were observed with WFCAM (Casali et al. 2007) on the 3.8-m UKIRT[2] on 2008 March 10/20 (ID: U/08A/32, PI: G. P. Smith). A total exposure time of 800 s pixel^{-1} was accumulated in both J and K bands using the same macrostepping (13-arcmin offsets in RA and Dec. to cover the large gaps between the detectors), jittering and 2×2 microstepping strategy used by the UKIDSS Deep Extragalactic Survey (DXS; Lawrence et al. 2007). The data were reduced and processed by the Cambridge Astronomical Survey Unit, and photometrically calibrated to the Vega magnitude system using Two Micron All Sky Survey (2MASS) stars in the fields. The final pixel scale of the UKIRT data is 0.2 arcsec pixel^{-1}; point sources detected in both filters have a full width at half-maximum (FWHM) of $\sim$1 arcsec.

We also make use of wide-field optical imaging from the 8.3-m Subaru Telescope.[3] These Suprime-CAM (Miyazaki et al. 2002) data (ID: S05A-159, PI: N. Okabe) have been used by Okabe & Umetsu (2008) to study the mass distribution of A1758 via the cluster's weak lensing signal – the weak lensing mass map from Okabe & Umetsu is reproduced in Fig. 1. Full details of the observations and data reduction are provided by Okabe & Umetsu. The reduced data consist of stacked g and $R_{\rm C}$ (hereafter R) exposures totalling 720 s in g and 2880 s in R. Point sources in both filters have FWHMs of $\sim$0.7 arcsec. Suprime-CAM's field of view is $34 \times 27\,{\rm arcmin^2}$ with a pixel scale of 0.206 arcsec pixel^{-1}. Both optical frames were registered on to the K-band frame using the IRAF tools GEOMAP and GEOTRAN. The transformations were defined by comparison of the positions of 100–300 sources in each image, and were found to be accurate to 0.1–0.15 arcsec across the whole field.

2.2 Archival XMM-LSS data

In Section 3.2 we use broad-band optical/NIR colours of 24-μm sources to identify them as likely cluster galaxies or not. These selection criteria are derived from analysis of archival data on the XMM-LSS field at $\alpha = 2^{\rm h}26^{\rm m}$, $\delta = -4^\circ.5$. This field was observed at the relevant wavelengths by SWIRE (24 μm; Lonsdale et al. 2003), UKIDSS DXS (J, K; Lawrence et al. 2007), the Canada–France–Hawaii Telescope (CFHT) Legacy Survey D1 field (*ugriz*) and the VIMOS VLT Deep Survey (VVDS; Le Fèvre et al. 2005).

The properties of the SWIRE data are similar to our own 24 μm discussed in Sections 2.1 and 3.1: an overall exposure time per pixel of 80 s, a final pixel scale of 1.2 arcsec and complete to $\sim$450 μJy. In our analysis we use the SWIRE XMM-LSS DR2 catalogue from the entire 9 deg^2 XMM-LSS field.[4] The UKIDSS DXS J/K-band data also match our data well, with total integration times of 640 s, the same macro- and microstepping strategy, the same final pixel-scale and comparable image quality of FWHM $\sim$ 0.9 arcsec. The final reduced UKIDSS DXS J/K-band frames were obtained from the UKIRT science archive. The CFHTLS D1 g/r-band frames were obtained from the CFHTLS Terapix First data release at the Canadian Astronomy Data Centre. These data have slightly worse image quality than Okabe & Umetsu's Subaru data (FWHM $\sim$ 0.9 arcsec) and are $\sim$0.5 mag deeper.

[1] This work is based in part on observations made with the *Spitzer Space Telescope*, which is operated by the Jet Propulsion Laboratory, California Institute of Technology under a contract with NASA (contract 1407).

[2] UKIRT is operated by the Joint Astronomy Centre on behalf of the Science and Technology Facilities Council of the United Kingdom.

[3] Based on data collected at the Subaru telescope, which is operated by the National Astronomical Observatory of Japan.

[4] The SWIRE XMM-LSS DR2 catalogue is available here: http://swire.ipac.caltech.edu/swire/astronomers/data_access.html

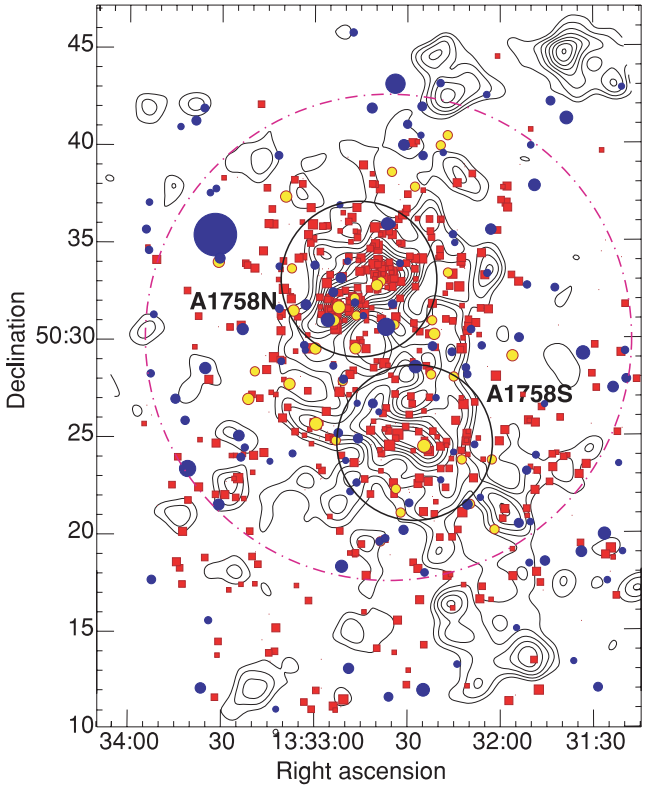

Figure 1. Spatial distribution of galaxies in the A1758 field whose $R'J'K'$ colours place them at the cluster redshift (see text). Red squares indicate passive spheroids ($n > 2.5$ and no 24 μm detection): the area of each symbol is proportional to the K-band flux. Yellow circles indicate passive spirals ($n < 2.5$ and no 24 μm detection). Blue circles indicate star-forming disc galaxies; the area of each symbol is proportional to the 24-μm flux. Overlaid are contours of the lensing κ-field reconstructed from weak shear data. The contours are spaced in units of 1σ reconstruction error. The two black circles indicate regions of 1-Mpc radius centred on A1758N and A1758S, while the magenta dot–dashed circle indicates the 12.5 arcmin (3 Mpc) radius region used to define the whole A1758 cluster population.

Crucially for the calibration of our photometric selection methods described in Section 3.2, a large spectroscopic redshift catalogue is available for the XMM-LSS field. The VIRMOS team obtained 8981 redshifts[5] down to a limit of $I_{AB} = 24$, of which 1543 correspond to $K < 19$ galaxies – i.e. brighter than $\sim 0.03 L^{\star}_{K}$ at $z = 0.28$. In Section 4 we consider only those with redshift quality flags of two or greater, indicating a >75 per cent confidence in the redshift.

3 PHOTOMETRIC ANALYSIS

3.1 Object detection and multicolour photometry

The 24-μm mosaic of A1758 was analysed with SExtractor (Bertin & Arnouts 1996); following SWIRE we estimated the flux of objects within an aperture of diameter 21 arcsec, and applied an aperture correction of 1.29. The flux detection limits and completeness of the mosaic were determined by individually inserting 500 simulated sources into the mosaic for a range of fluxes and determining their detection rate and recovered fluxes, using identical extraction procedures. The sources used in the simulations were formed by extracting isolated, high signal-to-noise ratio and unresolved sources from the mosaic itself. From these simulations, we estimate that the 90 per cent completeness limit of our 24-μm mosaic is 400 μJy.

The optical and NIR data on both A1758 and XMM-LSS were analysed with SExtractor (Bertin & Arnouts 1996) in two frame mode, such that objects were selected in the K band. The SExtractor MAG_AUTO magnitude was adopted for the K-band total magnitudes, and colours were measured from the $g/R/J/K$-band frames within 2 arcsec diameter apertures, after degrading the optical images to have the same FWHMs as the K-band data. Note that the XMM-LSS r-band photometry was transformed to R using the $(r - i)$ colour correction of Lupton.[6] The additional uncertainty introduced by this transformation is 0.0072 mag. These optical/NIR catalogues were then used to identify the optical/NIR counterpart of each 24-μm source in the A1758 and XMM-LSS catalogues, as the nearest K-band source (where one exists) within 5 arcsec of the 24-μm centroid. From the completeness simulations described above we expect the positional uncertainty of 24-μm sources to be ∼0.75 arcsec. In total 571 $S_{24\,\mu m} > 400$ μJy sources were detected in the MIPS mosaic of A1758. Of these 455 have galaxy counterparts with $K < 19$, 26 are stars and 90 have no $K < 19$ counterpart within 5 arcsec. These latter sources we assume to be at high redshifts.

3.2 Selection of cluster galaxies

Galaxy colours depend on a complex combination of star formation history, metallicity, redshift and dust extinction, whose effects are often difficult to disentangle, especially if only optical data are available. For example, it is particularly important to consider the reddening effects of dust when considering IR-luminous sources whose spectral energy distributions (SEDs) are likely to be strongly affected by dust obscuration. Fortunately, the SEDs of galaxies are much less affected by both ongoing star formation history and dust in the NIR than the optical; the $J - K$ colour varies by just ∼0.1 mag across the entire Hubble sequence. In contrast the $J - K$ colour increases monotonically with redshift to $z \gtrsim 0.5$, from $J - K \sim 0.9$ at $z = 0$ to $J - K \sim 1.6$ at $z \sim 0.5$. This NIR redshift–colour relationship can be seen in Fig. 2 – galaxies of a particular redshift lie along a single narrow colour–magnitude (C–M) relation, the slope of which is due to the mass–metallicity relation whereby galaxies become systematically more metal rich with mass (e.g. Tremonti et al. 2004). Note that we do not see a separate red sequence and blue cloud, due to the insensitivity of the $J - K$ colour to current SFR.

We exploit the fact that galaxies of a given redshift lie on such a narrow C–M relation to empirically removing the effects of metallicity on galaxy colour by fitting the slope of the C–M relation, and subtracting it out. We optimize this for the cluster redshift, selecting those $K < 19$ VVDS galaxies in the redshift range 0.254–0.304 (shown as large green symbols in the right-hand panel of Fig. 2) and fitting their $J - K/K$ and $R - J/K$ C–M relations using the biweight estimator, obtaining the following transforms:

$$(J - K)' = (J - K) + 0.075(K - 17.0),$$

$$(R - J)' = (R - J) + 0.10(K - 17.0).$$

We show the resulting $R'J'K'$ colour–colour plot for A1758 and XMM-LSS in Fig. 3. The robust separation of stars and galaxies in $R'J'K'$ colour space is striking; stars have much bluer $J' - K'$

[5] Available at http://cencosw.oamp.fr/VVDS/VVDS_DEEP.html

[6] http://www.sdss.org/dr6/algorithms/sdssUBVRITransform.html

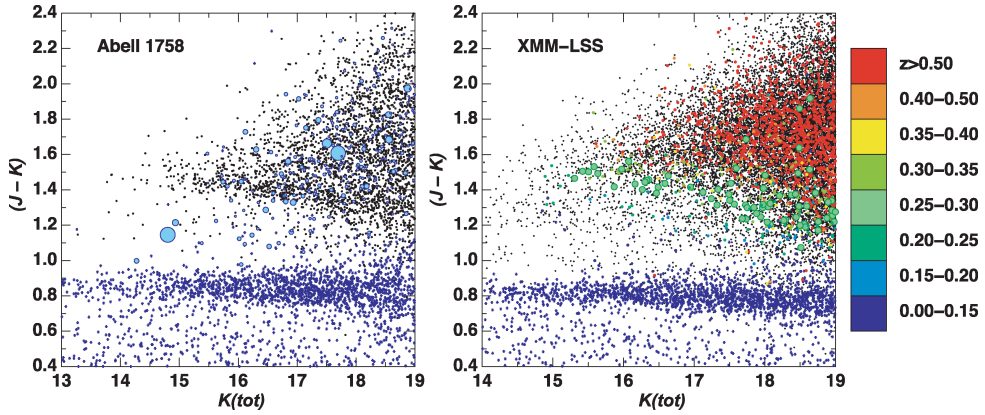

Figure 2. The $J - K/K$ C–M diagram of stars (blue stars) and galaxies (black points) in the Abell 1758 (left-hand panel) and XMM-LSS (right-hand panel) fields. In the left-hand panel those galaxies detected by *Spitzer* are indicated by light-blue circles, whose area is proportional to their 24-μm flux. In the right-hand panel galaxies with spectroscopic redshifts are indicated by symbols whose colour indicates their redshift from blue ($z < 0.2$) to red ($z > 0.5$) according to the key on the right. Those galaxies near the cluster redshift ($0.254 < z < 0.304$) are indicated by larger green symbols for emphasis.

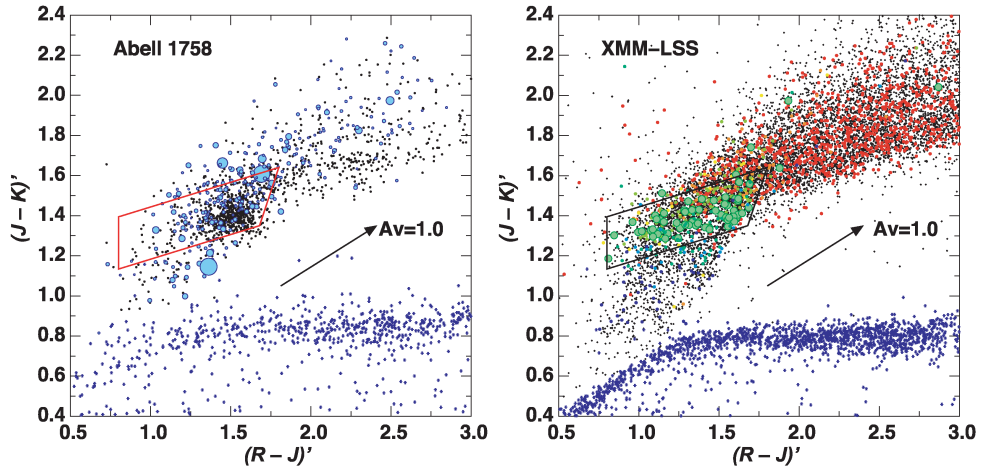

Figure 3. $R'J'K'$ colour–colour diagram of stars and galaxies in the A1758 cluster field (left-hand panel) and the XMM-LSS field (right-hand panel). The $(R - J)'$ and $(J - K)'$ colours are corrected to account for the slope of the C–M relation at $z \sim 0.3$ (see text). Symbols in the left- and right-hand panels are as for the corresponding panels in Fig. 2. The black/red box indicates the colour selection criteria used to identify galaxies at the cluster redshift. The black arrow indicates the effect of dust extinction at the level of $A_V = 1$ mag on galaxy colours.

colours than galaxies. The only overlap between stellar and galaxy loci is at $J' - K' \sim 0.8$, $R' - J' \sim 1.1$, i.e. for galaxies at $z \lesssim 0.1$ which are of no interest in this study. Star–galaxy separation is therefore achieved by selecting as galaxies objects with *either* extended morphologies *or* $R'J'K'$ colours outside the stellar locus. Using colour information to perform star–galaxy separation instead of a conventional extended versus unresolved morphological classification has the important advantage of removing the potential bias against very compact galaxies.

The large green symbols in the right-hand panel of Fig. 3 indicate those XMM-LSS galaxies at the cluster redshift ($0.254 < z < 0.304$), and can be seen to be well confined to a small region in the $R'J'K'$ colour space, and we use this to define a robust colour–colour selection criterion of

$$(R - J)' > 0.80,$$

$$(J - K)' > 0.94 + 0.24(R - J)',$$

$$(J - K)' > -2.71 + 2.42(R - J)',$$

$$(J - K)' < 1.20 + 0.25(R - J)',$$

as indicated in Fig. 3 by the black box.

We use the colours of those XMM-LSS galaxies with spectroscopic redshifts to estimate the completeness and purity of the galaxy sample selected using these colour cuts. We find that the completeness of the colour-selected sample is 90 ± 4 per cent – i.e. 90 per cent of XMM-LSS galaxies at $0.254 < z < 0.304$ satisfy the colour cuts. The sample has a purity of 31 ± 4 per cent – i.e. ∼30 per cent of the galaxies selected in this way actually lie at $0.254 < z < 0.304$. Varying the colour cuts would adjust the trade-off between completeness and purity. These colour cuts were chosen to optimize for completeness, with the impurity being addressed via a statistical contamination subtraction (Section 4.1). We find no evidence within the XMM-LSS data that we are missing dusty star-forming galaxies at the cluster redshift by not extending to redder $J' - K'$ or $R' - J'$ colours. Finally, we note that objects with blue optical–NIR colours ($R' - J' < 0.80$) are predominately quasars (not at the cluster redshift), hence necessitating the blue cut in $R' - J'$.

We therefore apply these colour cuts to the A1758 photometric catalogue, yielding 793 probable cluster members with $K < 18$ and within 3 Mpc of the cluster centre (left-hand panel of Fig. 3). Note that the observed concentration of galaxies with

$R' - J' \simeq 1.55$, $J' - K' \simeq 1.4$, corresponding to the early-type galaxies in A1758, provides independent confirmation of the validity of the colour selection criteria developed above from the XMM-LSS data. The angular distribution of galaxies selected to be likely cluster members in this manner is overplotted on the weak-lensing mass map in Fig. 1. Hereafter we refer to galaxies that satisfy the colour cuts developed in this section as 'cluster galaxies'.

We searched NASA/IPAC Extragalactic Database (NED)[7] for galaxies with spectroscopic redshifts within the Subaru field of view. Out of the 25 galaxies with redshifts, nine lie at $0.27 < z < 0.29$ and are therefore classified as cluster members. These nine include the BCG of both A1758N ($z = 0.2792$) and A1758S ($z = 0.2729$), but none of the galaxies that are detected at 24 μm. Nevertheless, all nine spectroscopically confirmed members satisfy our $R'J'K'$ colour selection criteria, confirming its high expected completeness. Moreover, all 11 of the galaxies with $z < 0.2$ were excluded from the cluster galaxy catalogue on the basis of having too blue $J - K$ colours, confirming our ability to remove foreground galaxies. We are less able to remove background galaxies, with five of seven galaxies with $0.32 < z < 0.48$ classed as probable cluster members, an issue also apparent from analysis of the VVDS galaxies in the XMM-LSS field. In future papers, we will have much more complete redshift information both for this cluster and the other 30 clusters in the LoCuSS sample, through a recently commenced large spectroscopic programme to obtain redshifts for 200–400 members per cluster.

4 RESULTS

4.1 Global properties

We now turn to the population of dust-obscured galaxies in A1758: 82 of the 793 probable cluster members have $S_{24\,\mu m} > 400\,\mu$Jy within 12.5 arcmin (3 Mpc) of the centre of A1758, producing a combined 24-μm flux of 85.8 mJy. We estimate the predicted contamination of field 24-μm sources by using the optical/NIR photometry of MIR sources from the SWIRE XMM-LSS survey. In total we identify 165 $K < 18$ sources with $S_{24\,\mu m} > 400\,\mu$Jy lying in the same $R' - J'$, $J' - K'$ selection box used to identify cluster members, within a total region of 2025 arcmin^2. Correcting for this level of field contamination, we report an excess of 42 MIR sources with $S_{24\,\mu m} > 400\,\mu$Jy, producing a combined flux of 42.7 ± 10.3 mJy. The uncertainty in this last value, and the global measurements that follow, is estimated by assuming each 24-μm source in the A1758 field has a probability of (42/82) of being a cluster member, and averaging over many Monte Carlo realizations of randomly selected cluster populations, such that the results are robust against any individual 24-μm source turning out to be a cluster member or not.

Our 24 μm flux limit of 400 μJy corresponds to average total IR luminosities of $5 \times 10^{10}\,L_\odot$ in A1758. This translates into a SFR of $\sim 8.5\,M_\odot\,yr^{-1}$, assuming the star formation calibration of Le Floc'h et al. (2005). They consider a range of SED templates to estimate the total IR luminosity, $L_{IR} = L(8\text{–}1000\,\mu m)$, of galaxies from their 24-μm flux, as a function of redshift. This calibration has a significant amount of scatter due to the range of possible IR SEDs, which at $z = 0.279$ corresponds to ∼0.1–0.2 dex. Integrating over all the 24-μm sources within 3 Mpc of the cluster centre, we estimate a global cluster SFR of $910 \pm 320\,M_\odot\,yr^{-1}$, including a 0.1 dex uncertainty in the overall SFR calibration. If we assign each individual cluster galaxy to either A1758N or A1758S based on proximity to the respective cluster centres, then the estimated SFR of each cluster is 580 ± 210 and $330 \pm 60\,M_\odot\,yr^{-1}$, respectively. Following Geach et al. (2006), we also divide our global cluster SFR by the cluster mass to estimate the specific star formation. Adopting the lensing results of Okabe & Umetsu (2008), we estimate that the mass of A1758, within the same $R < 3$ Mpc aperture used in this paper of $3.2 \pm 1.5 \times 10^{15}\,M_\odot$. This mass translates to a specific SFR of $29 \pm 16\,M_\odot\,yr^{-1}/10^{14}\,M_\odot$ placing A1758 among the more actively star-forming clusters (Fig. 4).

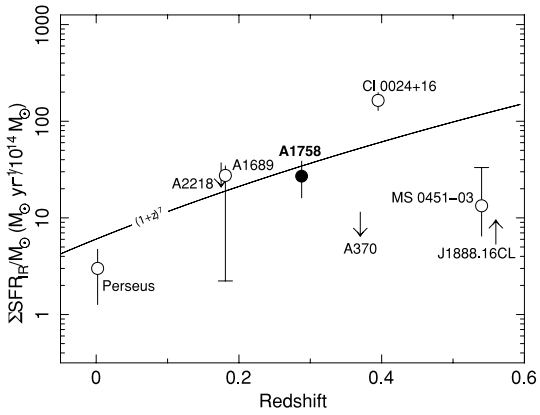

Figure 4. Variation in the specific SFR in clusters out to $z \sim 0.5$. The SFRs are from the MIR populations within ∼3 Mpc, and these are normalized to the best estimate of the cluster mass, derived by weak lensing estimates or from the X-ray luminosities. The solid point corresponds to the estimate for A1758. The errors are derived from bootstrap resampling of the MIR distribution. The open points and upper/lower limits for the remaining clusters are taken from Geach et al. (2006). Also plotted is an evolutionary model for the counts of star-forming ULIRGs from Cowie et al. (2004).

In the above estimates we have neglected the possible contribution from active galactic nuclei (AGN). We now investigate this by searching for X-ray point sources associated with the 24-μm sources in archive *XMM–Newton* and *Chandra* X-ray images, which cover both A1758N and A1758S (David & Kempner 2004; Okabe & Umetsu 2008), reaching sensitivities of $L_X(0.5\text{–}10\,keV) \sim 10^{41.5}\,erg\,s^{-1}$ at the cluster redshift. Among our 82 probable cluster members with $S_{24\,\mu m} > 400\,\mu$Jy we identify just two with coincident X-ray point sources, consistent with the typical X-ray selected AGN fractions in low-redshift ($z < 0.3$) clusters of 1–5 per cent (Martini et al. 2006; Silverman et al. 2009; Gallazzi et al. 2009). We note that this may be an underestimate of the AGN contamination, as many MIR-selected AGN are not detected in X-ray surveys (e.g. Hickox et al. 2009). In the future we will also be able to identify AGN from their optical spectra based on the emission-line ratios (Baldwin, Phillips & Terlevich 1981).

A final global measurement is the fraction of obscured star-forming galaxies in a manner analogous to the pioneering measurements of blue galaxy fractions by Butcher & Oemler (1978, 1984). The advantage of making these measurements in the MIR is that identifying galaxies as star forming solely on their optical colours is prone to underestimating the amount of star formation due to the obscuring effects of dust in the most actively star-forming galaxies. Following Saintonge et al. (2008), we estimate the fraction of cluster galaxies brighter than $M_B = -19.5$ and located within 1 Mpc of the cluster centre that are detected by MIPS, $f_{SF,MIPS}$, separately for the clusters A1758N and A1758S. For each cluster galaxy we derived rest-frame *B*-band absolute magnitudes and

[7] http://nedwww.ipac.caltech.edu/

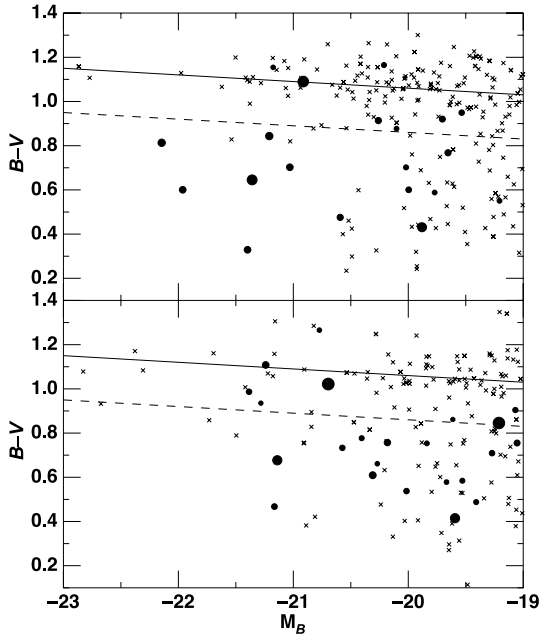

Figure 5. Rest-frame $B - V/M_B$ colour–magnitude diagrams for photometrically selected cluster members within 1 Mpc of Abell 1758N (top panel) and Abell 1758S (bottom panel). Black circles indicate those with $S_{24\,\mu m} > 400\,\mu$Jy, the area of each symbol being proportional to the 24-μm flux. Crosses indicate those galaxies not detected by *Spitzer*.

$B - V$ colours from the observed Subaru g and R-band magnitudes. Following Holden et al. (2007), this was done by deriving linear transformations from observed to rest-frame magnitudes for model galaxies at the cluster redshift covering a range of star formation histories, using the stellar evolution code of Bruzual & Charlot (2003). In Fig. 5 we show the resulting rest-frame $B - V/M_B$ colour–magnitude diagrams for cluster galaxies within 1 Mpc of A1758N and A1758S. Based on a comparison of source counts in these regions and the XMM-LSS field, we expect that field contamination to be at the level of one-in-10 for $M_B < -19.5$ galaxies, rising to one-in-four for those detected by *Spitzer*. We see that most 24-μm sources would also be classified as blue by the Butcher–Oemler criterion (i.e. blueward of the dashed line in each panel), but a significant fraction (∼20 per cent) of the star formation in A1758 comes from galaxies with colours consistent with those of early-type galaxies. Taking into account field galaxy contamination, we estimate the fraction of cluster galaxies brighter than $M_B = -19.5$ and located within 1 Mpc of the cluster centre that are detected by *Spitzer* (i.e. $S_{24\,\mu m} > 400\,\mu$Jy) to be (10 ± 3) per cent for A1758N, and (15 ± 4) per cent for A1758S (Fig. 6). By comparison to those galaxies in the XMM-LSS field satisfying the same colour selection criteria, we estimate that (28 ± 3) per cent of $M_B < -19.5$ (assuming that they are at $z = 0.28$) field galaxies at these redshifts have $S_{24\,\mu m} > 400\,\mu$Jy, somewhat higher than observed in the two clusters, as expected from the star formation–density relation (e.g. Lewis et al. 2002; Haines et al. 2007). We note that in terms of $f_{\rm SF,MIPS}$ A1758S appears the more active cluster, yet in terms of the global SFR, A1758N appears twice as active as A1758S, due primarily to A1758N being somewhat richer than A1758S.

4.2 Number counts

In Fig. 7 we show the differential number counts (solid black points) of 24-μm sources with $R'J'K'$ colours consistent with the cluster redshift and within 3 Mpc of the cluster centre. The open points show the differential 24-μm number counts after correcting for field galaxy contamination on the basis of the 24-μm sources in the XMM-LSS field satisfying the same colour selection, providing an estimate of the 24 μm luminosity function for A1758. According to this, almost all of the cluster 24-μm sources have $S_{24\,\mu m} < 1600\,\mu$Jy, which corresponds to a bolometric IR luminosity at $z = 0.279$ $L_{\rm IR} < 2 \times 10^{11}\,L_\odot$ based on the calibration of Le Floc'h et al. (2005). We estimate there to be 10 ± 6 LIRGs in Abell 1758, the same number as found for Cl 0024, although clearly without any redshift information this number is quite uncertain. We also identify one possible cluster ULIRG ($L_{\rm IR} > 10^{12}\,L_\odot$), which appears from the

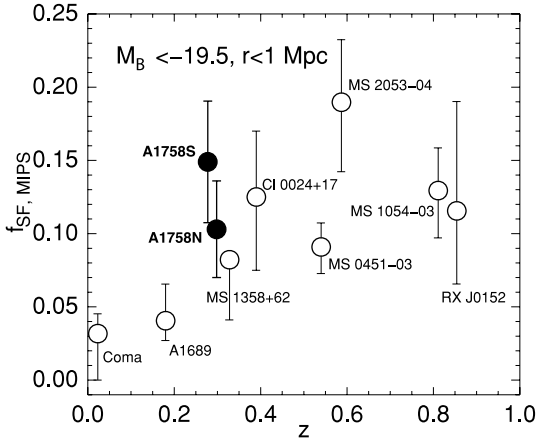

Figure 6. The MIR Butcher–Oemler effect. The fraction of $M_B < -19.5$ cluster galaxies within 1 Mpc of the cluster centre, that are star forming as revealed by the MIPS 24-μm observations, as a function of redshift. The solid symbols correspond to A1758N (lower) and A1758S (upper) at $z = 0.279$ and are offset slightly in z for clarity. The open symbols are taken from Saintonge et al. (2008).

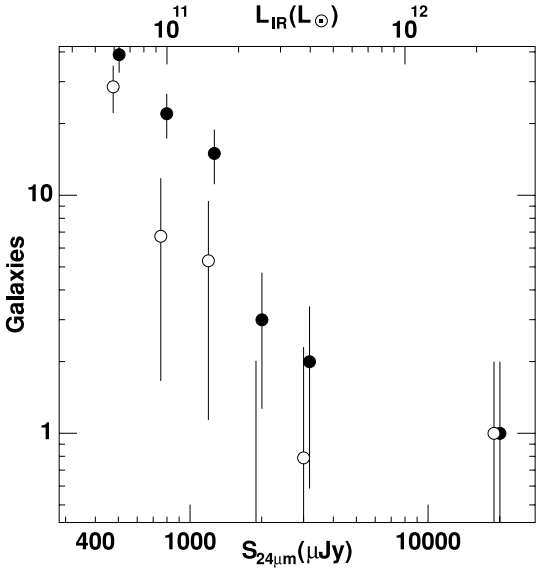

Figure 7. Number counts (filled symbols) and estimated luminosity function (open symbols) of 24-μm sources within 12.5 arcmin of the A1758 cluster centre, and whose $R'J'K'$ colours place them at the cluster redshift. The 24-μm luminosity function is based on statistical subtraction of 24-μm sources in the XMM-LSS field satisfying the same colour criterion. Scaled estimates of the bolometric IR luminosities, based on the calibration of Le Floc'h et al. (2005), are indicated along the top axis.

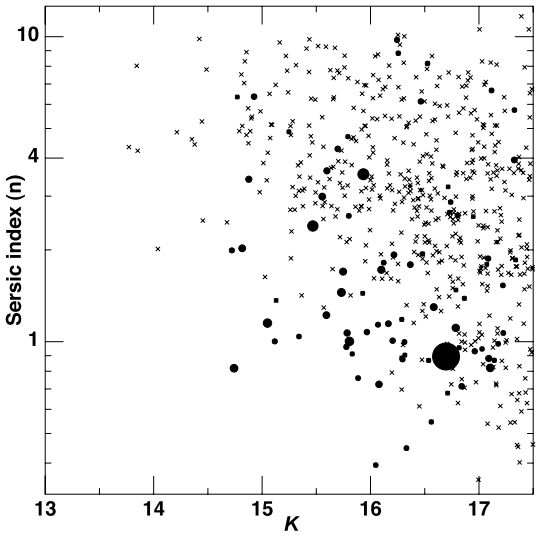

Figure 8. Morphologies and K-band magnitudes of those galaxies within 12.5 arcmin of the A1758 cluster centre whose *RJK* colours place them at the cluster redshift. Circles indicate galaxies detected with *Spitzer*, the area of each symbol is proportional to the 24-μm flux. Crosses indicate those galaxies not detected in 24 μm.

optical image to be a merging galaxy system with a combined NIR luminosity of $\sim$0.4 $L^{\star}_{K}$.

4.3 Surface photometry and morphology

We now turn to the morphology of the dust-obscured galaxies in A1758. Ideally this analysis would be based on wide-field high-resolution imaging with the *Hubble Space Telescope*, allowing detailed morphological classifications across the full field (e.g. Moran et al. 2007). In the absence of such data, we analyse the Subaru R-band frame, using 2DPHOT (La Barbera et al. 2008) to derive structural parameters for each cluster galaxy. 2DPHOT is an automated tool to obtain both integrated and surface photometry of galaxies, the main steps of which are (i) estimation of the FWHM and the robust identification of stars; (ii) construction of an accurate point spread function (PSF) model, taking into account both possible spatial variations as well as non-circularity; (iii) derivation of structural parameters (effective radius $r_{\rm e}$, mean surface brightness $\langle\mu\rangle_{\rm e}$ and Sersic index n) by fitting 2D PSF-convolved Sersic models to the data. The high-quality Subaru data, obtained in excellent conditions, allows us to obtain structural parameters accurate to $\delta n/n \sim 0.05$.

In Fig. 8 we plot Sersic index n versus K-band magnitude for all cluster members. Those galaxies detected by *Spitzer* are indicated by circles whose area is proportional to the 24-μm flux, while non-detections ($S_{24\,\mu{\rm m}} < 400$ μm) are shown as crosses. Sersic indices can be used to achieve a crude morphological classification into bulge- and disc-dominated galaxies (e.g. Driver et al. 2006; Ball, Loveday & Brunner 2008), and so adopting a nominal dividing line of $n = 2.5$ we classify the *Spitzer*-detected cluster galaxies as being either bulge dominated ($n > 2.5$) or disc dominated ($n < 2.5$). This yields the following fractions: $(26.8^{+11.1}_{-9.4})$ per cent of MIR-bright cluster galaxies are bulge dominated and $(73.2^{+9.4}_{-11.1})$ per cent are disc-dominated where the quoted uncertainties are 2σ binomial error bars following Gehrels (1986). The *Spitzer*-detected cluster galaxies are therefore dominated by disc galaxies, indeed many have large axis ratios which may suggest that some of the dust obscuration is caused by viewing these galaxies close to edge-on. However, we see no significant difference in the axis ratios between those disc galaxies detected by *Spitzer* and those not, which points against any major inclination effect. Although a quarter of MIR bright cluster galaxies are early-types, these galaxies contribute just (13 ± 4 per cent) of the total 24-μm flux estimated in Section 4.1. Hence, even if all of the 24-μm emission in these galaxies is due to AGN, they do not significantly effect our global SFR estimates in Section 4.1.

4.4 Spatial distribution

In Fig. 1 we overplot the spatial distribution of cluster galaxies in A1758 on the projected cluster mass distribution from Okabe & Umetsu (2008; black contours). The spatial distribution of cluster early-type galaxies (filled red squares) closely follow the underlying dark matter distribution. The cores of both of the merging components of A1758N (at $\alpha \simeq$ 13:32:50, $\delta \simeq$ 50:32 and $\alpha \simeq$ 13:32:40, $\delta \simeq$ 50:33.5 – see Section 5) are particularly dominated by early-type galaxies. Numerous mass peaks of lower significance (e.g. at $\alpha \simeq$ 13:33:30, $\delta \simeq$ 50:23; $\alpha \simeq$ 13:31:40, $\delta \simeq$ 50:23 and $\alpha \simeq$ 13:32:00, $\delta \simeq$ 50:21) also contain overdensities of early-type galaxies.

The distribution of dusty star-forming galaxies ($S_{24\,\mu{\rm m}} > 400$ μm; blue circles) is much less concentrated spatially than the early types, consistent with being an infalling population. An important caveat is that $\sim$50 per cent of these galaxies are probably field contaminants that should be randomly distributed across the field. Indeed, these field galaxies may help to explain the population of star-forming galaxies that are not associated with mass–overdensities in the weak-lensing mass map. On the other hand, most of the dusty galaxies are indeed associated with overdensities in the mass map. In addition to the population of dusty disc galaxies that are associated with mass–overdensities at large radii – presumably in-falling galaxy groups – we also find dusty disc galaxies occupying the central region (projected radii of $R \lesssim 500$ kpc) of A1758N. In contrast the central region of A1758S is completely devoid of dusty disc galaxies.

We also identify a third significant population of galaxies in A1758 – passive spiral galaxies, defined empirically by $K < 16.5$, $n < 2.5$ and undetected at 24 μm, i.e. $S_{24\,\mu{\rm m}} < 400$ μJy (yellow circles in Fig. 1). We identify 37 such galaxies all of which lie within 3 Mpc of the centre of either A1758N or A1758S. This population trace the underlying mass distribution very well, and appears to be more concentrated than the dusty spiral galaxies, but less concentrated than the early-type galaxy population. The apparent concentration of these objects towards the cluster centre suggests that these are a cluster population. This is confirmed by their relative rarity in field regions – we find a density of just $34 \pm 13\,{\rm deg}^2$ such galaxies in the XMM-LSS data, corresponding to an expected field contamination of just 4.3 ± 1.6 within a region of projected radius $R = 3$ Mpc.

To examine the relative concentrations of the three galaxy populations discussed above more quantitatively, we show in Fig. 9 the radial distributions of early-type galaxies, passive spirals and dusty star-forming galaxies in A1758, after correcting for field galaxy contamination. The number density of all three populations decreases with increasing projected clustercentric radius, confirming that all three are associated with the cluster. The distribution of late-type galaxies (whether detected or not at 24 μm) is less centrally concentrated than the distribution of early-type galaxies; the radial distributions of 24-μm-detected and undetected late-type galaxies are consistent with the errors out to $\sim$8 arcmin, however, at larger

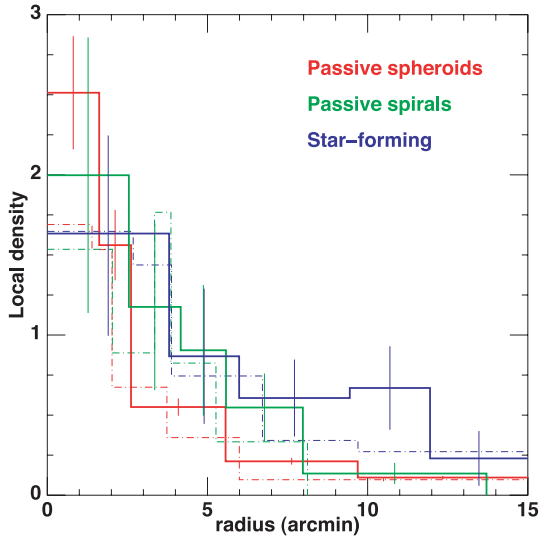

Figure 9. Comparison of the radial distributions of passive spheroids (red histograms), passive spirals (green histograms) and star-forming galaxies (blue histograms) in the A1758 cluster field. The solid histograms indicate clustercentric radii from just A1758N, while the dot–dashed histograms take the radius to be distance of each galaxy from the nearest of A1758N and A1758S. In each case, we correct the densities for field contamination based on the XMM-LSS field. The *y*-axis is an arbitrary density scale, normalized for ease of comparison between the galaxy populations.

radii there is an excess of 24-μm-detected galaxies over both early types and passive spirals. This excess corresponds to the galaxies discussed above that are associated with galaxy groups detected in the outskirts of the clusters in the weak-lensing map.

5 DISCUSSION

5.1 A1758 as a cluster merger – the mid-IR view

Okabe & Umetsu (2008) and David & Kempner (2004) have studied A1758 in detail as a merging cluster using weak lensing and X-ray data, respectively. In particular, David & Kempner investigated the thermodynamics of both cluster components. Here we compare our results on obscured star formation in A1758 with the thermodynamics of the ICM, and thus with the likely dynamical state of the cluster.

David & Kempner found no evidence of compressional heating of the ICM in the region between A1758N and A1758S, suggesting that the two clusters have not begun to merge with each other yet, although they may be gravitational bound to each other already. A1758N itself is interpreted as being a large impact parameter merger between two 7-keV clusters, one cluster (to the north-west) currently moving to the north and the other (to the south-east) currently moving to the south-east. In contrast, the merger in A1758S is interpreted as having a much smaller impact parameter with the merger occurring close to the line-of-sight through the cluster. The core radii of the merging components within A1758N are ∼100 kpc; in contrast the merging components of A1758S have core radii of 200 and 350 kpc. David & Kempner therefore suggested that, as a consequence of the differing impact parameters, the galaxies in the merging clusters of A1758S have experienced lower ram pressures than those in A1758N, and that A1758S may be at an earlier stage in its merger than A1758N. However, both A1758N and A1758S do contain regions of hotter gas that have presumably been shock-heated during the respective mergers. The precise timing difference between the two mergers is difficult to ascertain, however, David & Kempner (2004) proposed that A1758N is seen significantly after the point of closest approach whilst A1758S may be seen at approximately the epoch of closest approach. Okabe & Umetsu's weak lensing mass map successfully resolves the two merging components of A1758N, and locates a single mass peak in the core of A1758S, both of which are consistent with David & Kempner's interpretation of the X-ray data.

How well do our MIR results fit with the X-ray and lensing results? One of the most striking features of the distribution of obscured galaxies in Fig. 1 is their absence from the central $R \lesssim 500$ kpc region of A1758S, in contrast to the same region in A1758N, especially in the vicinity of the south-east component of A1758N. This difference between the clusters is reminiscent of the large cluster-to-cluster scatter within the core regions of merging clusters found with *ISO* (Metcalfe et al. 2005). Intense star formation can be triggered in cluster–cluster mergers by the passage of gas-rich galaxies through shocked regions of the ICM (Roettiger, Burns & Loken 1996). In A1758N the merger-induced shock-front(s) have dissipated (David & Kempner 2004), which helps to explain why shock-fronts are not found adjacent to the dusty galaxies in the core of that cluster. A1758S is claimed to be an earlier stage in the merging process, however, David & Kempner did detect shock-heated gas in this cluster. Therefore, naively one would expect that star formation would have been triggered by the shocks as in A1758N. However, no 24-μm sources are found in the central $R \lesssim 500$ kpc region of A1758S. The merger geometry of A1758S may help to explain the absence of obscured galaxies in its core. For example the 24-μm sources at $R \sim 500$–1000 kpc may have been scattered to large radii by the line-of-sight merger that is ongoing in the core of the cluster in a manner analogous to the distribution of cluster galaxies in Cl 0024, another line-of-sight merger cluster (Czoske et al. 2002). Assuming that the galaxies are moving at ∼1000 km s^{-1} it would take them ∼500 Myr to travel to a radius of $R \sim 500$ kpc from the centre of the cluster. On the face of it, this is inconsistent with David & Kempner's proposal that the subclusters in the A1758S merger are approximately at closest approach. An alternative interpretation of the 24-μm data might be that the shocks in A1758S were not strong enough to trigger detectable star formation in the cluster galaxies that passed though them. We also note that A1758S is much less optically rich than A1758N, so the absence of obscured activity in A1758S could simply be due to A1758S being a poorer cluster than A1758N. This is supported by Fig. 6 because the fraction of star-forming 24-μm-bright galaxies in both clusters is consistent within the errors.

In summary, our MIR results are qualitatively consistent with the previous X-ray and lensing results. However, the absence of obscured galaxies in the core of A1758S remains a puzzle. One possibility is that the galaxies were already gas poor before the cluster merger, and hence had no available fuel to undergo new star formation. Our results confirm and extend the view formed from *ISO* that the cluster-to-cluster scatter in merging clusters is large, and likely related to the physical parameters of cluster mergers.

5.2 Comparison with other clusters

The global SFR of A1758 estimated from the 24-μm flux of photometrically selected members is $910 \pm 320\,M_\odot\ yr^{-1}$, qualifying it as one of the most IR active clusters studied to date. For example it is comparable with the most active cluster studied to date –Cl 0024 at $z = 0.395$ with SFR $= 1000 \pm 210\,M_\odot\ yr^{-1}$ (Geach et al. 2006).

Globally this is unsurprising because A1758 contains two ongoing cluster–cluster mergers and one (between A1758N and A1758S) that may occur within a few Gyr.

However, the picture is more subtle when considering the specific SFR (Σ SFR) and star-forming fraction of galaxies ($f_{\rm SF,MIPS}$ – see Figs 4 and 6, respectively). Cl 0024 stands out in Fig. 4 as the most active cluster by a factor of $\sim$6 in Σ SFR because of its low mass relative to A1758. On the other hand, Cl 0024 and A1758 have comparable values of $f_{\rm SF,MIPS}$ (Fig. 6), indicative of the clusters having comparable optical richness. This further underlines the conclusion that numerous parameters influence the level of obscured star formation in galaxy clusters: merger geometry, density of the ICM, location of shock-heated gas with respect to the cluster galaxies, the available supply of gas in cluster galaxies in which star formation may be triggered by shock heating of the ICM, the optical richness of the cluster and cluster mass. We will investigate these issues in detail with the full sample in a future paper.

5.3 Passive spirals

We find a significant population of passive spiral galaxies, defined empirically by $K < 16.5$, $n < 2.5$ and $S_{24\,\mu\rm m} < 400\,\mu$Jy. The radial distribution of these galaxies is intermediate in radial extent between the cluster early types and the actively star-forming galaxies detected at 24 μm (Fig. 9). If the radial extent of each distribution indicates the length of time that each population has on average spent in the cluster potential well, then the passive spirals have been accreted by A1758 less recently than the actively star-forming galaxies. A simple interpretation is therefore that the passive spirals were formerly actively forming stars and thus brighter at 24 μm, i.e. that there is an evolutionary path linking the dusty star-forming galaxies, passive spirals and cluster early-type galaxies (see e.g. Wolf et al. 2009).

Moran et al. (2007) identified a significant population of passive spirals in Cl 0024 over a wide range of environments, and used a combination of *GALEX* UV photometry and optical spectroscopy to find that their star formation quenching time-scales are often > 1 Gyr, suggestive more of starvation, although the rapid quenching expected for ram-pressure stripping was also observed. As the simulations of Tonnesen, Bryan & van Gorkum (2007) show, gas is lost from infalling galaxies over a wide range of environments (even beyond the virial radius) on both short and long time-scales, and Moran et al. (2007) estimate that the observed frequency and quenching time-scales of passive spirals in $z \sim 0.4$ clusters could account for the entire build-up of S0s between $z = 0.4$ and 0.

The relationship between Moran et al.'s UV/optical selected passive spirals and our optical/IR selected passive spirals is currently unclear. For example, the evolutionary path outlined above may not include the UV/optical passive spirals discussed by Moran et al. (2007). On the other hand, if the two populations of passive spirals are indeed the same class of object, then the evolutionary path may not be valid. In that case an alternative interpretation of the differing radial distributions of dusty and passive spirals could be that the physical processes that trigger star formation in the former population are more efficient at the largest radii than the processes that act to quench star formation in the latter population. The *GALEX, Spitzer, Herschel*, ground-based NIR photometry and optical spectroscopy data set that we are assembling on a large sample of clusters will be very powerful for disentangling the respective galaxy populations.

6 CONCLUSIONS

We have presented the first results from our panoramic multiwavelength survey of 31 clusters at $z \simeq 0.2$ clusters as part of LoCuSS. For this initial study we chose A1758, an actively merging cluster at $z = 0.279$ that has been previously studied with high-quality weak lensing and X-ray data (David & Kempner 2004; Okabe & Umetsu 2008). Specifically, we have combined a wide-field ($25 \times 25\,{\rm arcmin}^2$) *Spitzer*/MIPS 24-$\mu$m map of the entire A1758N/A1758S complex with panoramic *J*/*K* band imaging from UKIRT/WFCAM and archival optical data from Subaru to map out the locations of dusty star-forming galaxies in addition to cluster early types and cluster spirals that are undetected down to $S_{24\,\mu\rm m} = 400\,\mu$Jy. The main results are as follows.

(i) We detect 82 probable cluster members in the MIR with *Spitzer*/MIPS at 24 μm within 3 Mpc of the cluster centre. After correcting for residual field contamination using archival data from the XMM-LSS, we measure an excess of 42 MIR sources over the field counts with $S_{24\,\mu\rm m} > 400\,\mu$Jy, responsible for a total flux of $S_{24\,\mu\rm m} = 42.7 \pm 10.3$ mJy.

(ii) Adopting Le Floc'h et al.'s (2005) SED templates, we convert our 90 per cent completeness limit of $S_{24\,\mu\rm m} = 400\,\mu$Jy into a luminosity sensitivity of $L_{8-1000\,\mu\rm m} \sim 5 \times 10^{10}\,{\rm L}_{\odot}$ – i.e. sub-LIRG luminosities. Most of the IR-luminous cluster sources appear to be sub-LIRGs. We estimate there to be 10 LIRGs within 3 Mpc of the cluster centre, comparable to the number in Cl 0024. We identify just one possible cluster ULIRG ($L_{\rm IR} > 10^{12}\,{\rm L}_{\odot}$), which appears to be a merging galaxy system with a combined NIR luminosity of $\sim 0.4 L_K^*$.

(iii) We also convert the total cluster flux at 24 μm to a total cluster SFR of ${\rm SFR_{IR}} = 910 \pm 320\,{\rm M}_{\odot}\,{\rm yr}^{-1}$. This is consistent within the errors with the most active cluster studied to date: Cl 0024 (Geach et al. 2006). We split the 24-μm sources between the A1758N and A1758S based the proximity of each galaxy to the respective cluster centres, to obtain ${\rm SFR_{IR}} = 580 \pm 210$ and $330 \pm 60\,{\rm M}_{\odot}\,{\rm yr}^{-1}$, respectively – i.e. A1758N is almost twice as active as A1758S.

(iv) When the level of obscured activity is normalized to the mass and the optical richness of the cluster, then we find that the specific SFR of A1758 is lower than that of Cl 0024 and that the fraction of cluster galaxies that are detected at 24 μm is comparable with Cl 0024. These results reflect the facts that A1758 is more massive than and of comparable richness to Cl 0024.

(v) Dust-obscured galaxies with late-type morphologies are detected in a network of infalling groups and filamentary structures that surround both A1758N and A1758S that is delineated by the reconstructed cluster mass distribution from Okabe & Umetsu (2008). However, in the core regions of each cluster we find that the central $R \lesssim 500$ kpc region of A1758N is comparatively rich in dusty galaxies in contrast to the absence of such objects in the same region of A1758S. This difference may be due to the differing recent dynamical histories of the two clusters, as discussed by David & Kempner (2004).

(vi) Finally, we identify a population of IR-selected passive spiral galaxies, i.e. they have a late-type morphology and are undetected at 24 μm. The radial distribution of these galaxies does not extend as far as that of the MIPS-detected population, suggesting that they were accreted into the cluster potential on average longer ago than the active dusty population. However, the difference in radial distribution may also indicates that they are a distinct population in transition from spiral to early-type morphology, and that they

are affected by different physical process than the dusty galaxies. Comparison of these IR passive spirals with UV-selected passive spirals will help to clarify the status of both populations.

The next steps in this study are to repeat this analysis for a large (∼20–30) sample of clusters in order to measure for the first time the scatter in the IR properties of clusters. The biggest caveat on our results is the reliance on photometry to select cluster galaxies. We will therefore also significantly enhance the precision of our analysis as spectroscopic redshifts become available from our ground-based optical spectroscopic observations recently commenced with Hectospec at the MMT. We also plan to integrate this optical/NIR/MIR analysis with our *GALEX* observations of the same clusters, and *Herschel* data when they become available. The overall goal is to pinpoint the contribution that the various physical processes make to the transformation of gas-rich spiral galaxies into early-type cluster galaxies via a large and detailed study of clusters in a single redshift slice.

ACKNOWLEDGMENTS

CPH and GPS acknowledge financial support from STFC. GPS and RSE acknowledge support from the Royal Society. We acknowledge NASA funding for this project under the *Spitzer* program GO:40872. We wish to thank the staff at UKIRT, CASU and WFAU for making the observations and rapidly processing the NIR data.

REFERENCES

Bai L. et al., 2007, ApJ, 664, 181
Baldwin A., Phillips M. M., Terlevich R., 1981, PASP, 93, 5
Ball N. M., Loveday J., Brunner R. J., 2008, MNRAS, 383, 907
Bertin E., Arnouts S., 1996, A&AS, 117, 393
Biviano A. et al., 2004, A&A, 425, 33
Böhringer H. et al., 2004, A&A, 425, 367
Boselli A., Gavazzi G., 2006, PASP, 118, 517
Bruzual G., Charlot S., 2003, MNRAS, 344, 1000
Butcher H., Oemler A., Jr, 1978, ApJ, 219, 18
Butcher H., Oemler A., Jr, 1984, ApJ, 285, 426
Caldwell N., Rose J. A., Sharples R. M., Ellis R. S., Bower R. G., 1993, AJ, 106, 473
Calzetti D. et al., 2007, ApJ, 666, 870
Casali M. et al., 2007, A&A, 467, 777
Coia D. et al., 2005a, A&A, 430, 59
Coia D. et al., 2005b, A&A, 431, 433
Cowie L. L., Barger A. J., Fomalont E. B., Capak P., 2004, ApJ, 603, L69
Czoske O., Moore B., Kneib J.-P., Soucail G., 2002, A&A, 386, 31
David L. P., Kempner J., 2004, ApJ, 613, 831
De Propris R., Stanford S. A., Eisenhardt P. R., Holden B. P., Rosati P., 2007, AJ, 133, 2209
Desai V. et al., 2007, ApJ, 660, 1151
Dressler A., 1980, ApJ, 236, 351
Dressler A. et al., 1997, ApJ, 490, 577
Dressler A., Rigby J., Oemler A., Jr, Fritz J., Poggianti B., Rieke G., Bai L., 2009, ApJ, 693, 140
Driver S. et al., 2006, MNRAS, 368, 414
Duc P.-A. et al., 2002, A&A, 382, 60
Duc P.-A. et al., 2004, in Diaferio A., ed., IAU Colloq. 195: Outskirts of Galaxy Clusters: Intense Life in the Suburbs. Cambridge Univ. Press, Cambridge, p. 347
Ebeling H., Edge A. C., Bohringer H., Allen S. W., Crawford C. S., Fabian A. C., Voges W., Huchra J. P., 1998, MNRAS, 301, 881
Ebeling H., Edge A. C., Allen S. W., Crawford C. S., Fabian A. C., Huchra J. P., 2000, MNRAS, 318, 333
Egami E. et al., 2006, ApJ, 647, 922
Fadda D., Elbaz D., Duc P.-A., Flores H., Franceschini A., Cesarsky C. J., Moorwood A. F. M., 2000, A&A, 361, 827
Gallazzi A. et al., 2009, ApJ, 690, 1883
Geach J. E. et al., 2006, ApJ, 649, 661
Gehrels N., 1986, ApJ, 303, 336
Gordon K. D. et al., 2005, PASP, 117, 503
Haines C. P., Gargiulo A., La Barbera F., Mercurio A., Merluzzi P., Busarello G., 2007, MNRAS, 381, 7
Haines C. P. et al., 2009, ApJ, submitted
Hickox R. C. et al., 2009, ApJ, 696, 891
Holden B. P. et al., 2007, ApJ, 670, 190
Kennicutt R. C., Jr et al., 2007, ApJ, 671, 333
Kneib J.-P., Ellis R. S., Smail I., Couch W. J., Sharples R. M., 1996, ApJ, 471, 643
La Barbera F., Carvalho R. R., Kohl-Moreira J. L., Gal R. L., Soares-Santos M., Capaccioli M., Santos R., Sant'Anna N., 2008, PASP, 120, 681
Lawrence A. et al., 2007, MNRAS, 379, 1599
Le Fèvre O. et al., 2005, A&A, 439, 845
Le Floc'h E. et al., 2005, ApJ, 632, 169
Lewis I. et al., 2002, MNRAS, 334, 673
Limousin M. et al., 2007, ApJ, 668, 643
Lonsdale C. et al., 2003, PASP, 115, 897
Marcillac D., Rigby J. R., Rieke G. H., Kelly D. M., 2007, ApJ, 654, 825
Martini P., Kelson D. D., Kim E., Mulchaey J. S., Athey A. A., 2006, ApJ, 644, 116
Metcalfe L. et al., 2003, A&A, 407, 791
Metcalfe L., Fadda D., Biviano A., 2005, Space Sci. Rev., 119, 425
Miller N. A., Owen F. N., 2003, AJ, 125, 2427
Miller N. A., Oegerle W. R., Hill J. M., 2006, AJ, 131, 2426
Miyazaki S. et al., 2002, PASJ, 54, 833
Moran S. M., Ellis R. S., Treu T., Smith G. P., Rich M. R., Smail I., 2007, ApJ, 671, 1503
Muzzin A., Wilson G., Lacy M., Yee H. K. C., Stanford S. A., 2008, ApJ, 686, 966
Navarro J. F., Frenk C. S., White S. D. M., 1997, ApJ, 490, 493
Okabe N., Umetsu K., 2008, PASJ, 60, 345
Okabe N., Takada M., Umetsu K., Futamase T., Smith G. P., 2009, preprint (arXiv:0903.1103)
Owen F., Ledlow M. J., Keel W. C., Morrison G. E., 1999, AJ, 118, 633
Poggianti B. M., Smail I., Dressler A., Couch W. J., Barger A. J., Butcher H., Ellis R. S., Oemler A., Jr, 1999, ApJ, 518, 576
Postman M. et al., 2005, ApJ, 623, 721
Rieke G. H. et al., 2004, ApJS, 154, 25
Roettiger K., Burns J. O., Loken C., 1996, ApJ, 473, 651
Saintonge A., Tran K.-V. H., Holden B. P., 2008, ApJ, 685, L113
Silverman J. D. et al., 2009, ApJ, 695, 171
Smail I., Morrison G., Gray M. E., Ower F. N., Ivison R. J., Kneib J.-P., Ellis R. S., 1999, ApJ, 525, 609
Smith G. P., Taylor J. E., 2008, ApJ, 682, L73
Smith G. P., Treu T., Ellis R. S., Moran S. M., Dressler A., 2005, ApJ, 620, 78
Swinbank A. M., Bower R. G., Smith G. P., Smail I., Kneib J.-P., Ellis R. S., Stark D. P., Bunker A. J., 2006, MNRAS, 368, 1631
Tanaka M., Kodama T., Arimoto N., Okamura S., Umetsu K., Shimasaku K., Tanaka I., Yamada T., 2005, MNRAS, 362, 268
Tomita A., Nakamura F. E., Takata T., Nakanishi K., Takeuchi T., Ohta K., 1996, AJ, 111, 42
Tonnesen S., Bryan G. L., van Gorkum J. H., 2007, ApJ, 671, 1434
Tremonti C. et al., 2004, ApJ, 613, 898
Treu T., Ellis R. S., Kneib J.-P., Dressler A., Smail I., Czoske O., Oemler A., Natarajar P., 2003, ApJ, 591, 53
Werner M. W. et al., 2004, ApJS, 154, 1
Wolf C. et al., 2009, MNRAS, 393, 1302
Zhang Y.-Y., Finoguenov A., Böhringer H., Kneib J.-P., Smith G. P., Kneissl R., Okabe N., Dahle H., 2008, A&A, 482, 451

This paper has been typeset from a TEX/LATEX file prepared by the author.